HHS Public Access

Author manuscript

Dev Cell. Author manuscript; available in PMC 2023 November 07.

Published in final edited form as:

Dev Cell. 2022 November 07; 57(21): 2483–2496.e4. doi:10.1016/j.devcel.2022.10.004.

A Scribble/Cdep/Rac pathway controls follower cell crawling and cluster cohesion during collective border cell migration

Joseph P. Campanale[1,2], **James A. Mondo**[1,2], **Denise J. Montell**[1,*]

[1]Molecular, Cellular and Developmental Biology Department, University of California Santa Barbara, Santa Barbara, CA 93106, USA.

[2]These authors contributed equally

Summary

Collective cell movements drive normal development and metastasis. *Drosophila* border cells move as a cluster of 6–10 cells, where the role of the Rac GTPase in migration was first established. In border cells, as in most migratory cells, Rac stimulates leading edge protrusion. Upstream Rac regulators in leaders have been identified; however, the regulation and function of Rac in follower border cells is unknown. Here we show that all border cells require Rac, which promotes follower cell motility and is important for cluster compactness and movement. We identify a Rac guanine nucleotide exchange factor, Cdep, that also regulates follower cell movement and cluster cohesion. Scribble, Discs Large, and Lethal Giant Larva localize Cdep basolaterally and share phenotypes with Cdep. Relocalization of Cdep::GFP partially rescues Scribble knockdown, suggesting that Cdep is a major downstream effector of basolateral proteins. Thus, a Scrib/Cdep/Rac pathway promotes cell crawling and coordinated, collective migration *in vivo*.

eTOC blurb

Collective migrations drive development and metastasis. While leader cells have commanded the most attention, Campanale and Mondo et al show in Drosophila border cells that followers are also essential. They find polarity proteins control the Rac-activator Cdep to stimulate F-actin dynamics to drive follower cell crawling behaviors and cluster cohesion.

Graphical Abstract

[*]Lead Contact: dmontell@ucsb.edu.

Author contributions

Conceptualization, J.P.C., J.A.M, and D.J.M.; Methodology J.P.C., J.A.M, and D.J.M.; Validation, J.P.C. and J.A.M; Formal Analysis, J.P.C. and J.A.M; Investigation, J.P.C. and J.A.M; Resources, J.P.C., J.A.M, and D.J.M.; Data Curation, J.P.C. and J.A.M; Writing - Original Draft, J.P.C., J.A.M, and D.J.M.; Writing - Review & Editing, J.P.C., J.A.M, and D.J.M.; Visualization, J.P.C. and J.A.M; Supervision, J.P.C., J.A.M, and D.J.M.; Funding Acquisition, J.P.C.and D.J.M.

Declaration of interests

The authors declare no competing interests.

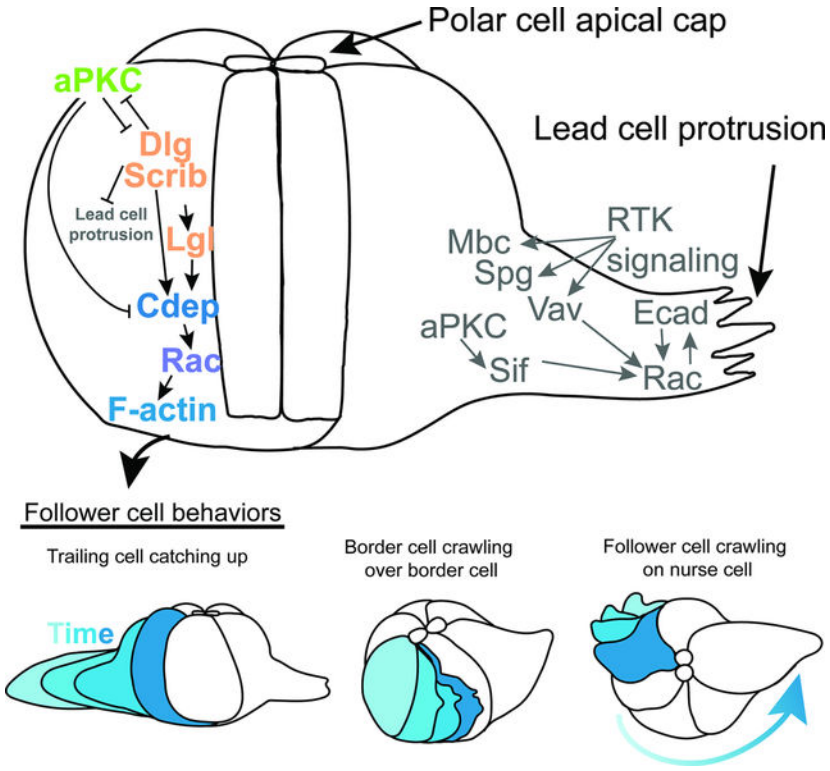

Keywords

Apicobasal polarity; Collective cell migration; RhoGTPases; Scribble complex; Par complex; Rac1; FARP2; Cdep; Border cells

Introduction

Collective cell migrations drive homeostasis, normal development, and tumor metastasis [1–5]. Within collectives, leaders and followers can be distinguished by their positions, and cells at the front typically steer the group [6–8]. Migrating cell collectives are diverse. They can be composed of sheets of hundreds of cells or clusters of a few cells. Recent work shows that circulating tumor cell clusters seed new metastases more effectively than single cells [9–14]. Thus, elucidating the mechanisms by which cell clusters move collectively is of particular interest.

The border cells in the *Drosophila* ovary have emerged as a powerful model for elucidating the cellular and molecular mechanisms regulating collective migration in general and cluster movement in particular [15–17]. *Drosophila* egg chambers consist of 15 nurse cells and one oocyte surrounded by a monolayer of follicle cells (Fig. 1A). Follicle cells exhibit classical epithelial polarity with apical microvilli, E-cadherin rich adherens junctions, lateral membranes, and basal surfaces, which contact a basement membrane that surrounds each follicle (Fig. 1A). During developmental stage 9, 6–10 anterior follicle cells called border cells delaminate as a cluster, detach from the basement membrane and their epithelial

neighbors, retain apicobasal polarity, and squeeze between the nurse cells to migrate to the oocyte [17] (Fig. 1A).

The evolutionarily conserved Rho family of small GTPases, Rac, Cdc42 and Rho, regulate the actin cytoskeleton dynamics that drive single and collective cell migrations *in vivo* and *in vitro* [18–21]. The *Drosophila* genome encodes three Rac genes, Rac1, Rac2 and Mig-2-like (Mtl), which in border cells promote lead cell protrusion and migration [22,23]. Rac activity is highest in the lead cell, and photoactivation of Rac in one cell is sufficient to make it the leader and steer the whole cluster [24].

Decades of research have focused on Rac activity and function in lead cell protrusions [22,23,25–28]. These large protrusions have at least two functions. First, they steer the cluster by sensing chemoattractants and small open spaces between nurse cells [29] and second, they facilitate mechanical communication by inhibiting large, outwardly directed lead-cell-like protrusions in follower cells [30]. However neither the contribution of follower cells to cluster motility nor the regulation and function of Rac in follower cells has been addressed. Follower cell behavior is generally a less well understood feature of collective cell migration, particularly *in vivo* [31].

Here we show that Rac is required in all cells of the border cell cluster and identify a basally localized Rac GEF, Cdep, that is required for follower cell crawling. We further show that Cdep membrane localization requires the basolateral proteins Scribble (Scrib), Discs Large (Dlg) and Lethal Giant Larva (Lgl). Inhibition of any of these components leads to defective cell motility and reduced cluster cohesion. This work suggests an integrated model of collective border cell migration in which guidance receptors activate Rac to stimulate lead cell protrusions that steer the cluster whereas basolaterally localized Cdep regulates Rac-dependent crawling in all cells to promote coordinated and cohesive movement.

Results

Rac is active and required in follower cells

To investigate the contribution of follower border cells to cluster migration, we performed timelapse imaging of delaminating clusters using markers for the two cell types that make up the cluster: a central pair of non-migratory polar cells, surrounded and carried by migratory cells [reviewed in [17]] (Fig. 1B–B”’, Movie 1). Live imaging of border cell F-actin at high spatial and temporal resolution showed that as the migratory cells round up and encase the polar cells, multiple cells generate large forward directed protrusions (Fig. 1B, Movie 1) and appear to compete to lead the cluster. Eventually, one cell “wins” (Fig. 1B’), and both the leader and followers move away from the epithelium (Fig. 1B’–1B”’).

The dominant negative form of Rac, Rac^{T17N} (RacDN), inhibits all three, functionally redundant, Racs in *Drosophila*. Expressing RacDN in all outer migratory cells blocks lead cell protrusion, cluster delamination and migration so the cells remain at the anterior tip of the egg chamber [22,23] (Fig. 1C). Using a RacFRET activity reporter, we observed that Rac activity in the lead cell is on average 15% higher than the rear. Rac is nearly as active in follower cells as in leader cells (Fig. 1D and E), and much more active in followers than in

non-motile polar cells (Fig. 1D); however its role in followers, if any, has not been addressed (Fig. 1F). Similarly, the regulatory network of guanine nucleotide exchange factors (GEFs) that activate Rac in the lead cell have been described (Fig. 1F), whereas the regulation of Rac in follower cells remains unexplored.

To test for the requirement for Rac in follower cells, we expressed RacDN clonally in a varying number of border cells using the FLP-OUT technique. We reasoned that if every cell contributes to cluster movement, then as more cells within the cluster express RacDN, we expect a concomitant decrease in cluster motility. So, we compared migration of clusters with different numbers of cells expressing UAS-MoesinGFP and either a control (UAS-*white* RNAi) or UAS-RacDN. All clusters containing cells expressing *white* RNAi completed migration by stage 10, regardless of the number of labeled cells (Fig 1G). In contrast, the more RacDN-expressing cells in a cluster, the more severe the migration defect (Fig. 1G). None of the clusters with four RacDN-expressing cells completed migration, and even a single RacDN-expressing cell could prevent completion of migration by stage 10 in 10% of clusters. We conclude that Rac activity in every migratory cell of the cluster contributes to their collective movement.

In contrast, inhibition of the receptor tyrosine kinases PVR and EGFR, which function redundantly upstream of Rac in lead cell protrusions [27], were not required in follower cells (Fig. 1G). Expression of dominant-negative PVR and EGFR (PVRDN and EGFRDN) in all border cells causes severe migration defects, and over-expression of PVR biases cells to assume the lead position [32]. However we found that PVR and EGFR activities were not required in follower cells (Fig. 1G). We conclude that there must be different upstream regulation of Rac in follower cells.

Rac is required for follower cell crawling behaviors

Since all cells contribute to cluster movement and require Rac, we carried out live imaging to assess what features of follower cell morphology and behavior Rac regulates. Live imaging of control clusters expressing MoesinGFP to label cortical F-actin revealed dynamic changes in follower cell shapes and significant movement toward the oocyte (Movie 2 and Fig. 2A). In contrast, clusters expressing RacDN were immobile over many hours (Movie 2 and Fig. 2B). Further imaging of control clusters (Fig. 2C) showed that when a follower cell trailed behind, it crawled forward to catch up to the rest of the cluster (Movie 3), and this behavior promoted cluster compactness (Fig. 2C'–C""). Careful examination of control movies revealed evidence for follower cell crawling throughout migration. For example, clusters move forward even during and after retraction of a lead cell protrusion (Movie 3, and Supplementary Fig. 1A), driven by follower cell motility. Near the end of migration, all cells often extend small basal protrusions and crawl simultaneously as the cluster advances (Movie 3 and Supplementary Fig. 1B). All such dynamic cell behaviors were absent from Rac inhibited clusters (Movie 2 and Fig. 2B).

While lead cell protrusions are obvious when the entire border cell cluster is labeled, follower cell morphology and dynamics are more challenging to discern due to the normally compact morphology of the cluster. Therefore we expressed MoesinGFP in subsets of border cells and made time lapse movies. Using the FLP-OUT technique, control clones expressing

MoesinGFP and RNAi against the *white* gene showed that follower cells typically extend dynamic protrusions and actively crawl over other cells of the cluster (Movie 4 and Fig. 2D–D””). In contrast, RacDN-expressing cells exhibit virtually no actin dynamics (Movie 4 and Fig. 2E–E””). In fixed imaging, we observed that labeled control follower cells typically exhibit a relatively compact morphology while extending lateral protrusions around E-cadherin boundaries with neighboring cells, enwrapping one another (Fig 2F, F’ and additional example in Movie 5).

In contrast, RacDN-expressing follower cells, which were most commonly in the rearmost position, failed to move (Fig. 2E–E””) and often developed an elongated morphology such that the majority of the cell lacked contact with and was not integrated into the cluster (Fig 2G, G’ and another example in Movie 5). This elongated morphology was only observed in mixed clusters that include migratory wild type cells. We never observed elongated morphology in clusters in which all cells express RacDN (Fig. 2B). We conclude that the wild type cells drag the immobile, RacDN-expressing cell(s), which are unable to move forward and catch up the way that wild type cells do if they fall behind (Fig. 2C’–C””).

Quantitative fluorescence microscopy revealed reduced levels of cortical F-actin in Rac inhibited follower cells relative to controls (Fig. 2H). Moreover, even when only one or two cells lacked Rac activity, the velocity of the whole cluster was reduced ~2-fold (Fig. 2I), providing further evidence that each cell requires Rac to contribute to cluster movement (Fig. 1G). These results demonstrate that Rac promotes F-actin dynamics and follower cell motility, which is required for cluster movement.

Clonal labeling of cells with MoesinGFP also revealed that follower cells normally change shape over time (Fig. 2J–J””) whereas RacDN-expressing cells exhibit little or no change in shape over long periods, whether they had a compact or elongated shape (Fig. 2K–K” and Supplementary Fig. 2). In contrast, follower cells expressing PVRDN and EGFRDN were indistinguishable from wild type: they changed shape dynamically and were not elongated (Fig. 2L). We conclude that follower cells require Rac for F-actin polymerization and dynamics, cell shape changes, and motility which promote cluster compactness and movement, independent of EGFR and PVR.

The basally localized RacGEF, Cdep, is required for follower cell crawling and cluster cohesion

The Rac GEFs Sponge (Spg), myoblast city (Mbc), and Vav are required downstream of EGFR and PVR in the lead cell for protrusion [25,26,33]. To determine which GEF(s) might be required in follower cells, we carried out an RNAi screen of 26 putative Rho family GEFs and identified one, Cdep, that is required for the crawling behavior of follower border cells. In contrast to control clusters, which move as a compact and cohesive unit (Movie 6, Fig. 3A), Cdep RNAi-expressing border cell clusters do not (Movie 6, Fig. 3B and Supplementary Fig. 3). Two different RNAi lines effectively knocked down Cdep protein (Supplementary Fig. 3A–B’) and caused similar defects. *Cdep* is the predicted *Drosophila* ortholog of human FARP1 (FERM, ARH/RhoGEF And Pleckstrin Domain Protein 1) (29% identical and 42% similar) and *FARP2* (27% identical and 40% similar).

Wild type border cells initiate migration with a single, large, lead cell protrusion, and when individual frames taken at ~30 minute intervals from a time lapse movie are displayed in different colors in a single figure, the spatial separation between border cell clusters at different time points reflects cohesive, coordinated, and efficient cluster movement (Fig. 3A). The crawling defect in Cdep knockdown clusters (Movie 6) causes abnormally elongated clusters (Fig. 3B and Supplementary Fig. 3D–L). Similar to RacDN clones, some cells of the cluster do not crawl forward (Movie 6). The white color in Fig. 3B indicates overlap of multiple time points and thus failure to move. Cluster cohesion was reduced and some cells protruded ectopically (Fig. 3B, arrows).

In fixed imaging, we also observed trailing cells and split clusters consistent with an inability of the follower cells to crawl on one another to maintain cluster cohesion (Fig. 3C–G). In some cases a single cell showed a trailing phenotype similar to clonal expression of RacDN in a single cell (Fig. 3C, C'), while in other cases a single cell detached from the cluster (Fig. 3E). Interestingly, such cells could make a lead-cell-like protrusion (Fig. 3E). The trailing phenotype and separation of follower cells caused an increase in the cluster aspect ratio in Cdep knockdown clusters (Fig. 3H).

Cdep, FARP1 and FARP2 contain DH (Dbl homology) and PH (pleckstrin homology) domains that define the Dbl family of Rho family GEFs [34]. FARP1 and FARP2 are *bona fide* Rac GEFs [34,35] and can activate Cdc42 in some cell types [36]. To determine whether *Cdep* is a RacGEF in border cells, we expressed *Cdep* or control RNAi for the *yellow* (*y*) or *w* gene in combination with a validated RacFRET activity probe [24]. Indeed, knockdown of *Cdep* with two independent RNAi constructs modestly but significantly lowered RacFRET but not Cdc42FRET compared to the controls, indicating *Cdep* is a *bona fide* RacGEF in border cells (Fig. 3I). The effect of Cdep is impressive considering that at least four Rac GEFs function redundantly in lead cell protrusions. Interestingly, while overall levels of RacFRET were reduced in Cdep knockdown clusters, the front-back bias of Rac activity was unchanged (Fig. 3J and K), supporting the hypothesis that Cdep functions predominantly outside of the lead cell protrusion.

To gain further insight into Cdep function, we examined its localization. We found that an endogenously GFP-tagged Cdep (Cdep::GFP) is expressed in all follicle cells, including border cells (Fig. 3L–P). Co-staining with the cell adhesion molecule E-cadherin, which is enriched in subapical adherens junctions, showed that Cdep localizes to basolateral membranes in the follicular epithelium (Fig. 3M) and in border cell clusters (Fig 3N–P). Cdep::GFP is enriched at cell-cell contacts but not in lead cell protrusions (3N). High resolution imaging of migrating clusters showed that Cdep is particularly enriched basally at polar/border cell contacts (Fig. 3O) and at border/border cell membranes (Fig. 3P).

Apicobasal polarity proteins regulate Cdep localization

Epithelial follicle cells exhibit classical apicobasal polarity with apically localized atypical protein kinase C (aPKC), lateral Scrib, and a basal basement membrane (Fig 4A and B). Border cells retain some apicobasal polarity as they migrate [37,38]. However, polarity is clearest in contacts between polar cells and between border cells and polar cells (Fig. 4C). As border cells delaminate, they undergo a 90° turn, which causes the apical domain to

orient roughly perpendicular to the direction of migration (Fig. 4D–F"). At the end of migration, they turn again to dock their apical surfaces to the oocyte (Fig. 4G–G"). The basolateral protein Scrib is found on basal and lateral membranes between border cells and polar cells and the apical polarity determinant, aPKC, is enriched in apical junctions (Fig. 4B, C). Crumbs, Par, and Scrib modules are required for border cell migration [33,38–41], but the mechanism by which they act is not yet clear.

To interrogate the relationship between Cdep and the polarity modules, we compared Cdep localization to that of aPKC, the Scrib module, and the basal kinase Par-1. Cdep::GFP membrane localization partially overlapped with Par-1 (Fig. 4H, Supplementary Fig. 4A–A"'), although Cdep was concentrated even more basally than Par-1 in these cells. Cdep was undetectable in apical membranes and thus did not colocalize with aPKC at the polar cell/border cell boundary. Cdep overlaps with Scribble in lateral membranes though Cdep is concentrated more basally, while Scrib is most enriched just basal to the adherens junction (Fig. 4I and Supplementary Fig. 4B–B"').

To test if Cdep membrane localization and polarization depends on apicobasal polarity proteins, we examined Cdep::GFP in cells expressing RNAi lines against *Par-1*, *aPKC*, and *scrib*. Par-1 knockdown did not detectably change the localization of GFP::Cdep (Fig. 4K). In contrast, knockdown of either Scrib or aPKC caused a general reduction in Cdep::GFP membrane association and a more diffuse cytoplasmic signal (Fig. 4L and M). Line scans of border cell-polar cell contacts from basal to apical showed that Par-1 knockdown did not change Cdep asymmetry whereas Scrib and aPKC did (Fig. 4N and O). Dlg and Lgl knockdowns phenocopied Scrib (Fig. 4O).

Analysis of posterior epithelial follicle cells from the same egg chambers also showed a difference in Cdep membrane localization. Knockdown of either Scrib or aPKC causes multiple layers of follicle cells to form, characteristic of epithelial polarity defects (Fig. 4P–R). Whereas Cdep::GFP is normally excluded from apical domains (Fig. 4P, P'), Cdep was present on all cell surfaces within the layering event and was enriched between layers (Fig. 4Q, Q'). Conversely, knockdown of Scrib led to reduced membrane accumulation of Cdep::GFP on lateral membranes and more diffuse cytoplasmic signal (Fig. 4R–R'). The data from both border cells and posterior follicle cells suggest that the Scrib module promotes Cdep membrane association whereas aPKC antagonizes it.

A prediction then is that expression of a constitutively active form of aPKC would reduce Cdep membrane association. As expected, when we overexpressed a constitutively active form of aPKC lacking its NH_2-terminus (aPKCΔN) [42], Cdep::GFP failed to associate with basal membranes and appeared more diffusely cytoplasmic in both border cells (Fig. 4S and T) and epithelial cells (Supplementary Fig 4C and D). We conclude that the Scrib module promotes membrane association while aPKC excludes Cdep from the apical domain.

The Scrib module promotes cluster integrity independent of tumor suppression.

To investigate the mechanism by which Scrib, Dlg, and Lgl regulate border cell migration, we used validated RNAi lines to knock down their expression. However these proteins are tumor suppressors, loss of which causes hyperproliferation and multilayering of follicle

cells that at best complicate and at worst preclude analysis of border cell migration [43,44]. To circumvent this issue, we conditionally expressed RNAi lines targeting *scrib*, *dlg* or *lgl* using c306Gal4 [45] combined with the temperature-sensitive repressor tubGal80^{ts}. RNAi against the *white* gene was used as a control. Incubating c306Gal4, *tub*Gal80^{ts}, UAS-RNAi flies at 30°C (to inactivate Gal80^{ts}) for 72 hours was long enough to achieve knockdown of Scrib, Dlg and Lgl (Supplementary Fig. 5A–F) without causing multilayering or proliferative tumors. Compared to control clusters, knockdown of the Scrib module reduced the percentage of border cells that complete migration (Supplementary Fig. 5G–H). Multiple RNAi lines against each gene caused similar effects (Supplementary Fig. 5H). Longer incubation times resulted in multilayering, as expected (Supplementary Fig. 5I–K).

To gain insight into what the Scribble module regulates in border cells we evaluated clusters expressing RNAi in combination with LifeActGFP. These analyses revealed that the Scribble module is required for cluster cohesion (Fig. 5), similar to Cdep. Live imaging showed that in contrast to controls (Fig. 5A, Movie 7), Scrib, Dlg or Lgl knockdown caused clusters to elongate as they migrated (Fig. 5B–D, Movie 7), and increased overall cluster aspect ratios by ~50% (Fig. 5E).

High resolution snapshots of fixed cluster morphology showed that in contrast to cohesive control border cell clusters at stage 9 with a single lead cell protrusion (Fig. 5F), knockdown of Scrib, Dlg or Lgl caused individual cells to split off (Fig. 5G, H, red arrows), and abnormally large, leader-like protrusions from follower cells (Fig. 5G–I, orange arrows). In the most extreme cases of cluster cohesion loss, individual cells separated from the cluster (Supplementary Fig. 5L–S). To quantify this phenotype, we clonally knocked down Scrib in cells of the cluster and observed that ~40% of *scrib* RNAi containing clusters had cells that completely detached from their neighboring wild type counterparts compared to ~5% in *white* RNAi (Fig 5L). These results indicate that Scrib knockdown impedes migration and reduces cluster cohesion.

Since Scrib module proteins are required for Cdep localization and Cdep is a RacGEF Rac, we might expect Scrib knockdown to cause a similar reduction in Rac activity. However, Scrib knockdown also causes a more severe cluster cohesion phenotype and more frequent and larger, lead cell-like protrusions, which could reflect increased Rac activity in follower cells. To determine the effect of Scrib on Rac, we measured Rac activity in Scrib or Dlg knockdown cells, we found a loss of asymmetry in Rac activity but no change in total FRET (Fig. 5K–M). Thus the basolateral complex has multiple functions in border cells, one of which is to localize Cdep to basolateral membranes and another is to suppress lead cell protrusions in follower cells, similar to Cdc42 [46], the moesin kinase misshapen [47], and moesin itself [28] (see discussion).

Localizing Cdep to basal membranes partially suppresses Scrib phenotypes

Scrib knockdown causes diverse phenotypic effects and Scrib interacts with dozens of binding partners [48], raising the question as to which effectors mediate Scrib function. Since Scrib knockdown disrupts Cdep membrane localization, we wondered which, if any, Scrib functions Cdep might mediate. So we used the GrabFP system to relocalize Cdep::GFP to basal membranes in Scrib knockdown cells. GrabFP is an anti-GFP nanobody-based trap

that was developed to concentrate GFP tagged proteins in specific subcellular locations [49]. We used GrabFP-Basal, in which Nrv1 is fused to the anti-GFP nanobody to target it to basolateral membranes. As a negative control we used ExGrabFP-Basal, in which the anti-GFP nanobody is expressed on the exterior of the cell and so should not interact with intracellular Cdep. We expressed either GrabFP-Basal or ExGrabFP-Basal with Cdep::GFP and UAS-*scrib* RNAi with c306Gal4 in the absence of tubGal80^{ts}. Without tubGal80^{ts} to attenuate the Scrib knockdown phenotype, egg chambers had extensive anterior follicle cell layering (Fig 6A and D, white arrows) in addition to border cell migration phenotypes (Fig 6B and E) and elongation of the border cell cluster (Fig 6C and F). Under these conditions, most egg chambers eventually became necrotic (Fig. 6D), hampering our ability to quantify border cell motility. However, expression of GrabFP-Basal efficiently restored basolateral localization of Cdep::GFP in *scrib* RNAi-expressing follicle cells (Fig. 6A–C). Basolateral localization of Cdep::GFP also ameliorated multiple Scrib knockdown phenotypes including egg chamber death (Fig 6A and D) and follicle cell layering frequency and severity (Fig. 6G and H) compared to the ExGrabFP-Basal control. In the healthy stage 10 egg chambers, we observed a significant reduction in the number of anterior layering events with GrabFP-Basal vs ExGrabFP-Basal (Fig. 6I). Cluster cohesion was also significantly improved in GrabFP-Basal vs ExGrabFP-Basal (Fig. 6J). We conclude that basolateral membrane targeting of Cdep is sufficient to improve egg chamber viability, restore follicle cell epithelial polarity, and promote border cell cluster cohesion.

To test whether basolateral localization of Cdep is essential for its function in border cells, we combined Cdep::GFP with GrabFP-Apical in otherwise wild type border cells. Apical targeting of Cdep caused incomplete border cell migration in 50% of clusters compared to less than 5% of control clusters expressing GrabFP-Basal (Fig. 6K–M). These data support the conclusion that Cdep localization to basolateral membranes is essential for its normal function in border cell migration.

In further support of the sufficiency of basolateral Cdep to rescue epithelial follicle cell defects, we found that basolaterally localized Cdep also reduced the frequency of ovariole strands containing even a single egg chamber of any stage with any epithelial layering (Fig. 6G). In addition, even in those egg chambers that did have multiple layers, basolateral re-localization of Cdep significantly reduced the number of cell layers (Fig. 6H) ($p<.0001$). These findings suggest that a major function of the Scrib module during egg chamber development is to localize Cdep to basolateral membranes.

Discussion

Collective cell migration is a widespread phenomenon that drives much of embryonic development, wound healing, and tumor metastasis. In migrating collectives, there are typically leader cells that extend protrusions outward from the group to steer it [7,8,50,51]. The functions of follower cells are less clear [31], especially *in vivo*. Follower cell contributions have primarily been studied in collective sheet migration *in vitro*, rather than in small clusters. But clusters are emerging as major contributors to metastasis [9–11,52,53], so it is of interest to understand the mechanisms by which clusters maintain cohesion as they move.

Cohesion of collectively migrating cell sheets has been attributed to cadherin-mediated adhesion between cells [7]. In border cells, as in collective sheet migration, Ecadherin mechanically couples leaders to followers [30], inhibiting followers from generating large outward protrusions between nurse cells. However, E-cadherin knockdown in outer border cells does not cause a loss of cluster cohesion; rather the clusters lack a leader and tumble in random directions [30].

Based on the data presented here, we propose that border cell cluster cohesion is mediated at least in part by follower cells enwrapping one another and crawling over one another as the cluster moves, a behavior with some resemblance to a “rolling swarm” of caterpillars [54]. Followers maintain cohesion of the swarm by crawling on each other while forward movement is achieved by a combination of crawling on the substrate and over one another. Similarly, we propose that border cells maintain cohesion by crawling on each other, movements that likely drive reported leader exchanges [55] and cluster tumbling [56]. We further propose that the cluster moves forward by a combination of crawling on nurse cells and over one another.

In many ways the E-cadherin knockdown phenotype and the Scrib/Cdep knockdown phenotypes are complementary to one another. In E-cadherin knockdowns, cluster cohesion is maintained and follower cells are active, while lead cell protrusions are lost (Fig 7 of this work and Cai et al., 2014, Figure 1F, Movie S2). Conversely, in Scrib or Cdep knockdowns, leading protrusions are present, but follower cells are impaired in motility, so that the cluster becomes elongated, and some cells completely detach.

In border cells, the lead cell protrusion was initially proposed to function as a grapple that would pull the rest of the cluster forward [57,58]. This idea implied that the follower cells might be passive passengers, thus much work focused on elucidating the molecular pathways regulating Rac in the lead cell protrusion. However the grapple model was based on fixed tissue imaging.

Live imaging has revealed that 90% of lead protrusions retract and that cluster speed is uncorrelated with extension or retraction of lead protrusions [59]. These observations lead to a model in which the large forward-directed protrusion is primarily a sensory structure, probing for chemoattractants, traction, and physical spaces, rather than a grapple [29].

If the lead protrusion does not function as a grapple, then how does the cluster actually move? Here we show that all cells contribute to cluster movement. Previous work noted that non-leader cells produce small protrusions between nurse cells, three times smaller on average than lead cell protrusions [47]; however neither the origin nor function of these protrusions has been addressed. We show that Rac is required in each cell for all F-actin dynamics including small outward protrusions on the nurse cell substrate and dynamic protrusions of one border cell over another.

Eukaryotic cell crawling typically requires cycles of protrusion at the front, adhesion to a substrate, and actomyosin-mediated contraction to pull up the rear [60–65], although the relative importance and sequence of these events can vary [66,67]. RacDN-expressing border cells are excluded from lead positions, exhibit reduced cortical F-actin, and are essentially

immobile. Interestingly, a single RacDN-expressing cell frequently exhibits an elongated morphology, which appears to result from their inability to crawl forward to keep up with the rest of the cluster. Since the overall levels of cortical F-actin are reduced, this phenotype may be due to impaired protrusion, cortical contractility, or both.

In contrast to Rac, the chemoattractant receptors are only required in the lead cell, so the molecular pathway regulating Rac-mediated follower cell crawling differs from the regulators of lead cell protrusion. Here we show that the basolateral proteins Scrib, Dlg and Lgl localize Cdep to promote Rac-dependent follower cell motility. Scrib, Dlg, and Lgl have additional functions in addition to the pathway described here, so their knockdown causes additional phenotypes including disinhibition of lead cell protrusions in follower cells. This phenotype resembles that caused by knockdown of a number of other proteins including Cdc42 [46], the moesin kinase misshapen [47], and moesin itself [28], which supports the cell cortex by binding cortical F-actin to the plasma membrane. One possibility is that the basolateral complex functions in a common pathway with these proteins to restrict leader cell protrusions.

Scrib, Dlg and Lgl are best known as tumor suppressors [68–70], mutation of which causes tissue overgrowth. Scrib loss of function causes epithelial to mesenchymal transition and increased single cell invasion in cells expressing oncogenic Ras [71–73]. Paradoxically though, Scrib, Dlg, and Lgl are infrequently mutated in human cancers [74,75]. The results here provide a possible explanation. We show that Scrib loss of function impedes collective motility of border cell clusters. If tumors spread collectively and Scrib is similarly required for cluster cohesion and coordinated migration, then the function identified here could provide a selective pressure against Scrib loss-of-function mutations.

Polarity signaling complexes and Rho GTPase activities appear to be well-conserved between border cells and mammalian cells that migrate collectively, and a basal Rac GEF dependent upon Scribble has even been predicted but not yet identified [60]. The results presented here suggest that FARP1 and FARP2 would be excellent candidates to mediate cluster cohesion in collectively migrating mammalian cell clusters downstream of Scribble. Neither has been extensively studied, however the little that has been reported is intriguing. *FARP1* is required for migration of lung adenocarcinoma cells [34], and *FARP2* promotes collective invasion of colorectal carcinoma [76]. Colorectal carcinomas invade and spread as small groups of cells with apicobasal polarity. It will be interesting to determine whether it serves a similar function in that context.

Limitations of the Study

One limitation of the study is that, while Rac is clearly required for follower cell protrusion and motility, it may have additional functions such as supporting the F-actin cortex that contribute to the observed phenotypes. This Study identifies a single RacGEF required in follower cells. It is likely that additional GEFs and GAPs are required. The Gal4 used in this study is expressed in both border and polar cells. It is an open question if polarity module proteins have both cell autonomous and non-autonomous functions. Whether the mechanisms described here are general to other cell types remains to be determined.

STAR Methods

RESOURCE AVAILABILITY

Lead Contact—Further information and requests for resources and reagents should be directed to and will be fulfilled by the Lead Contact, Denise Montell (dmontell@ucsb.edu).

Materials Availability—*Drosophila* lines and other reagents generated in this study will be available upon request.

Data and Code Availability—Data including all raw image files in this study will be made available upon request.

EXPERIMENTAL MODEL AND SUBJECT DETAILS

***Drosophila* husbandry and genetics—**Standard cornmeal-yeast food (https://bdsc.indiana.edu/information/recipes/molassesfood.html) was used to grow all fly strains used in this study. All vials of flies contained at least 5mL fly food. Flies were kept in incubators at 25°C, 80% humidity and on a 12 hr light/dark cycle unless otherwise noted.

A detailed list of all fly strains used in this study and their source can be found in key resources table. Genotypes for every figure panel can be found in supplementary table 1. Most crosses were grown at 25°C and flies were fattened by yeast addition on an *ad libitum* basis for three days at 29°C before dissection. The exceptions were for crosses containing the conditional expression construct, tubGal80ts, in which flies were grown at 18°C and transitioned to 30°C for fattening. tubGal80ts is a temperature dependent repressor of Gal4 activity, thus at restrictive temperature (18°C) Gal4 remains inactive and at permissive temperature (30°C), Gal80ts is inactive therefore allowing Gal4 to be active. Experiments that required clonal border cells expressing RNAi and a fluorescent clonal marker were generated using the FLP/FRT clonal marking system [77]. RNAi stocks were crossed to either hsp70-FLP; Acty17bGal4, UAS-moesin-GFP or hsp70-FLP; Tub[FRT]CD2[FRT]Gal4, UAS-GFP/SM5a were heat-shocked two times at 37°C with at least 6 hours between each heat shock. Flies were fattened for 48 hr and dissected as stated below for fixed staining or live imaging.

METHOD DETAILS

Immunohistochemistry

5–7 fattened adult female flies were dissected in Schneider's Medium (ThermoFisher, catalog #21720001) supplemented with 20% fetal bovine serum and 1x antimycotic/antibiotic (VWR, catalog #45000–616). Ovarioles were separated from the muscle sheath using Dumont style 5 stainless steel forceps (Electron Microscopy Sciences) before fixation. Egg chambers were fixed in 4% paraformaldehyde in phosphate buffered saline (PBS) for a total of 15 min at room temperature before washing three times 15 min with PBS+0.2% TritonX-100 (PBST). Primary antibodies were diluted in PBST and ovarioles were incubated overnight at 4°C. Egg chambers were then washed with PBST three times at room temperature, incubated in fluorescently conjugated secondary antibodies (Invitrogen, all

AlexaFluor conjugated goat antibodies) in PBST for 2 hr, and washed three times more with PBST. Samples were then mounted in VectaShield (Vector Laboratories, catalog #H-1000) mounting medium and stored at 4°C until imaging. Egg chambers were mounted on a #1.5 coverglass and imaged with either a Zeiss LSM780 or LSM800 confocal microscope using either a PlanAPO 20× 1.2NA, PlanAPO 40× 1.4NA or a LD LCI Plan-Apochromat 63xW 1.2NA. All image settings were kept exactly the same within each experiment.

Antibodies used in this study include: rabbit anti-Scrib (kind gift from Dr. Chris Doe, 1:2000), guinea pig anti-Scrib (kind gift from Dr. David Bilder, 1:500), Rabbit anti-Par-1 (a kind gift from Dr. Jocelyn McDonald, 1:500), mouse anti-PKCζ (sc-216) and rabbit anti-PKCζ (sc-17781), and rabbit anti-LGL (sc-9826) were from Santa Cruz Biotechnology and used at 1:500, mouse anti-Dlg (4F3, 1:25), mouse anti-Cut (2B10, 1:100) and rat anti-Ecad (DEcad, 1:20) were from the Developmental Studies Hybridoma Bank, rabbit anti-GFP (A11122, 1:1000) from ThermoFisher, chicken anti-GFP (ab13970, 1:1000) from Abcam. Lectin PNA Alexa 647 was purchased from Thermo Fisher Scientific (L32460).

Live imaging

Egg chambers were dissected from 5–7 fattened adult female flies in Schneider's Medium supplemented with 20% fetal bovine serum and 1x antimycotic/antibiotic. Egg chambers were washed two times with dissecting medium and mounted on Lumox imaging dishes in medium containing 0.4 mg/mL bovine insulin and 1% low melt agarose. Egg chambers were imaged by confocal as above.

QUANTIFICATION AND STATISTICAL ANALYSIS

Generation of Imaris reconstructions (Movie 5):

Images first had gaussian smoothing applied to all channels. The Imaris Surface function was then used to segment the individual channels.

Quantification of apical-basal polarization of proteins along the border cell-polar cell boundary (Figure 4J–O):

When possible the apical cap of the polar cells was identified by either E-cadherin, Phalloidin/F-actin or aPKC staining. Using ImageJ a line scan with a thickness of .75 μm was drawn tracing the border cell-polar cell boundary using the F-actin channel as a guide. Measurements were then taken in the Cdep channel and averaged over 0.50 μm to smooth the signal and then normalized to the peak value within an individual border cell cluster. Representative line scans were chosen for the line graphs. To compare population differences we took the average of the 25% most basal signal divided by the 25% most apical signal for each sample. This ratiometric measurement of basal asymmetry was used for statistics and population level plotting. In a subset of polarity complex knockdown samples the apical cap could not be easily distinguished and an arbitrary pole was chosen as basal. In this condition, there was no bias seen in Cdep asymmetry regardless of orientation or start point chosen.

Quantification cluster aspect ratio (Figures 3H and 5E): A bounding box was manually drawn in FIJI around the border cell cluster in an anterior-posterior orientation. The aspect ratio of the bounding rectangle was then measured and plotted for each condition.

Quantification of cluster speed (Figure 2I):

The center of mass of the border cell cluster was manually identified in each time point. The MTrackJ plugin was then used to calculate the velocity of the border cell cluster.

Quantification of Rac FRET (Figure 3I):

FRET images were obtained during live cell imaging on a Zeiss LSM 780. A 458-nm laser was used for excitation of the sample. CFP and YFP images were collected simultaneously using channel 1 (464–502 nm) and channel 2 (517–570 nm) under a 40×/1.1 numerical aperture (NA) water immersion objective LD C-Apo lens. Images were taken at 16-bits with a frame size of 512 × 512 in the center of mass of the border cell cluster. CFP and YFP images were then processed using Fiji image analysis software as described before [78]. The final FRET image of the YFP/CFP ratio image was generated in ImageJ. The average FRET signal of the entire cluster was measured. All samples were observed after detachment and prior to docking. FRET index was measured by splitting the cluster into thirds along the anterior-posterior axis and dividing the posterior third by the anterior most third.

Quantification of layering (Figure 6H–I):

Images were taken of whole ovariale strands at a low zoom-level on a 20x objective using a Zeiss LSM 800 or Zeiss LSM 780. Images were 30–36 microns in thickness with a z-step of 2.5–3 microns. Images were then manually quantified in ImageJ by observing any location within the follicular epithelium that showed layering in any stage egg chamber. Quantification of layering was done only on anterior layering events in stage eight and nine egg chambers. The distance from the anterior tip of the egg chamber to the posterior-most cell within the layering event was measured to quantify the size of the layering event.

Quantification of cluster length (Fig 6J):

Cluster length was measured in Fiji. A line scan was drawn to the longest axis of the border cell cluster in the anterior to posterior orientation. If measuring a cluster that had split apart, measurements went from the anterior tip of the fallen off cell to the posterior tip of the lead cell of the cluster.

ADDITIONAL RESOURCES

All data were analyzed in Excel (Microsoft). Graphs and statistics were generated in Prism 9 (GraphPad). For statistical analysis by one-way ANOVA, Bartlett's Test was run to determine if significant differences in sample deviations warranted non-parametric analysis. In cases where deviations were not significantly different, parametric ANOVA was performed with Tukey post-hoc tests of significance. In cases where deviations were found to be significantly different, non-parametric ANOVA was run with Kruskal-Wallace post-hoc tests of significance. All bar graphs contain the N for that experiment over the respective bar.

Supplementary Material

Refer to Web version on PubMed Central for supplementary material.

Acknowledgments

We would like to acknowledge Dr. Lauren Penfield for Movie 2. We thank Drs. Lauren Penfield, Abhinava Mishra, Wei Dai, Guangxia Miao, and Allison Gabbert for thoughtful discussions. We acknowledge the use of the NRI-MCDB microscopy facility at UC Santa Barbara. We thank Drs. David Bilder and Christopher Doe for *Drosophila* Scrib antibody and Dr. Jocelyn McDonald for Par-1 antibody. We acknowledge the Bloomington Drosophila Stock Center and Vienna Drosophila Resource Center for fly stocks. This work was funded by an American Cancer Society award PF-17-024-01-CSM to J.P.C and an NIH grant R01GM46425 to D.J.M.

References

1. Friedl P, and Gilmour D (2009). Collective cell migration in morphogenesis, regeneration and cancer. Nat. Rev. Mol. Cell Biol. 10, 445–457. 10.1038/nrm2720. [PubMed: 19546857]
2. Friedl P, Sahai E, Weiss S, and Yamada KM (2012). New dimensions in cell migration. Nat. Rev. Mol. Cell Biol. 13, 743–747. 10.1038/nrm3459. [PubMed: 23072889]
3. Scarpa E, and Mayor R (2016). Collective cell migration in development. J. Cell Biol. 212, 143–155. 10.1083/jcb.201508047. [PubMed: 26783298]
4. Mishra AK, Campanale JP, Mondo JA, and Montell DJ (2019). Cell interactions in collective cell migration. Development 146. 10.1242/dev.172056.
5. Stuellton C, Parent CA, and Montell DJ (2017). Cell Motility in Cancer Metastasis: Mechanistic Insights from Simple Model Organisms. NRC.
6. Revenu C, Streichan S, Donà E, Lecaudey V, Hufnagel L, and Gilmour D (2014). Quantitative cell polarity imaging defines leader-to-follower transitions during collective migration and the key role of microtubule-dependent adherens junction formation. Development 141, 1282–1291. 10.1242/dev.101675. [PubMed: 24595289]
7. Khalil AA, and de Rooij J (2019). Cadherin mechanotransduction in leader-follower cell specification during collective migration. Exp. Cell Res. 376, 86–91. 10.1016/j.yexcr.2019.01.006. [PubMed: 30633881]
8. Zhang J, Goliwas KF, Wang W, Taufalele PV, Bordeleau F, and Reinhart-King CA (2019). Energetic regulation of coordinated leader-follower dynamics during collective invasion of breast cancer cells. Proc Natl Acad Sci USA 116, 7867–7872. 10.1073/pnas.1809964116. [PubMed: 30923113]
9. Aceto N, Bardia A, Miyamoto DT, Donaldson MC, Wittner BS, Spencer JA, Yu M, Pely A, Engstrom A, Zhu H, et al. (2014). Circulating tumor cell clusters are oligoclonal precursors of breast cancer metastasis. Cell 158, 1110–1122. 10.1016/j.cell.2014.07.013. [PubMed: 25171411]
10. Cheung KJ, and Ewald AJ (2016). A collective route to metastasis: Seeding by tumor cell clusters. Science 352, 167–169. 10.1126/science.aaf6546. [PubMed: 27124449]
11. Au SH, Storey BD, Moore JC, Tang Q, Chen Y-L, Javaid S, Sarioglu AF, Sullivan R, Madden MW, O'Keefe R, et al. (2016). Clusters of circulating tumor cells traverse capillary-sized vessels. Proc Natl Acad Sci USA 113, 4947–4952. 10.1073/pnas.1524448113. [PubMed: 27091969]
12. Campbell NR, Rao A, Hunter MV, Sznurkowska MK, Briker L, Zhang M, Baron M, Heilmann S, Deforet M, Kenny C, et al. (2021). Cooperation between melanoma cell states promotes metastasis through heterotypic cluster formation. Dev. Cell 56, 2808–2825.e10. 10.1016/j.devcel.2021.08.018. [PubMed: 34529939]
13. Kok SY, Oshima H, Takahashi K, Nakayama M, Murakami K, Ueda HR, Miyazono K, and Oshima M (2021). Malignant subclone drives metastasis of genetically and phenotypically heterogenous cell clusters through fibrotic niche generation. Nat. Commun. 12, 863. 10.1038/s41467-021-21160-0. [PubMed: 33558489]
14. Allen TA, Asad D, Amu E, Hensley MT, Cores J, Vandergriff A, Tang J, Dinh P-U, Shen D, Qiao L, et al. (2019). Circulating tumor cells exit circulation while maintaining multicellularity, augmenting metastatic potential. J. Cell Sci. 132. 10.1242/jcs.231563.

15. SenGupta S, Parent CA, and Bear JE (2021). The principles of directed cell migration. Nat. Rev. Mol. Cell Biol. 22, 529–547. 10.1038/s41580-021-00366-6. [PubMed: 33990789]
16. Norden C, and Lecaudey V (2019). Collective cell migration: general themes and new paradigms. Curr. Opin. Genet. Dev. 57, 54–60. 10.1016/j.gde.2019.06.013. [PubMed: 31430686]
17. Montell DJ, Yoon WH, and Starz-Gaiano M (2012). Group choreography: mechanisms orchestrating the collective movement of border cells. Nat. Rev. Mol. Cell Biol. 13, 631–645. 10.1038/nrm3433. [PubMed: 23000794]
18. Ridley AJ (2015). Rho GTPase signalling in cell migration. Curr. Opin. Cell Biol. 36, 103–112. 10.1016/j.ceb.2015.08.005. [PubMed: 26363959]
19. Lyda JK, Tan ZL, Rajah A, Momi A, Mackay L, Brown CM, and Khadra A (2019). Rac activation is key to cell motility and directionality: An experimental and modelling investigation. Comput. Struct. Biotechnol. J. 17, 1436–1452. 10.1016/j.csbj.2019.10.002. [PubMed: 31871589]
20. Nobes CD, and Hall A (1995). Rho, rac, and cdc42 GTPases regulate the assembly of multimolecular focal complexes associated with actin stress fibers, lamellipodia, and filopodia. Cell 81, 53–62. 10.1016/0092-8674(95)90370-4. [PubMed: 7536630]
21. Parri M, and Chiarugi P (2010). Rac and Rho GTPases in cancer cell motility control. Cell Commun. Signal. 8, 23. 10.1186/1478-811X-8-23. [PubMed: 20822528]
22. Murphy AM, and Montell DJ (1996). Cell type-specific roles for Cdc42, Rac, and RhoL in Drosophila oogenesis. J. Cell Biol. 133, 617–630. 10.1083/jcb.133.3.617. [PubMed: 8636236]
23. Geisbrecht ER, and Montell DJ (2004). A role for Drosophila IAP1-mediated caspase inhibition in Rac-dependent cell migration. Cell 118, 111–125. 10.1016/j.cell.2004.06.020. [PubMed: 15242648]
24. Wang X, He L, Wu YI, Hahn KM, and Montell DJ (2010). Light-mediated activation reveals a key role for Rac in collective guidance of cell movement in vivo. Nat. Cell Biol. 12, 591–597. 10.1038/ncb2061. [PubMed: 20473296]
25. Fernández-Espartero CH, Ramel D, Farago M, Malartre M, Luque CM, Limanovich S, Katzav S, Emery G, and Martín-Bermudo MD (2013). GTP exchange factor Vav regulates guided cell migration by coupling guidance receptor signalling to local Rac activation. J. Cell Sci. 126, 2285–2293. 10.1242/jcs.124438. [PubMed: 23525006]
26. Bianco A, Poukkula M, Cliffe A, Mathieu J, Luque CM, Fulga TA, and Rørth P (2007). Two distinct modes of guidance signalling during collective migration of border cells. Nature 448, 362–365. 10.1038/nature05965. [PubMed: 17637670]
27. Duchek P, Somogyi K, Jékely G, Beccari S, and Rørth P (2001). Guidance of cell migration by the Drosophila PDGF/VEGF receptor. Cell 107, 17–26. 10.1016/s0092-8674(01)00502-5. [PubMed: 11595182]
28. Ramel D, Wang X, Laflamme C, Montell DJ, and Emery G (2013). Rab11 regulates cell-cell communication during collective cell movements. Nat. Cell Biol. 15, 317–324. 10.1038/ncb2681. [PubMed: 23376974]
29. Dai W, Guo X, Cao YS, Mondo JA, Campanale JP, Montell BJ, Burrous H, Streichan S, Gov N, Rappel W-J, et al. (2020). Tissue topography steers migrating Drosophila border cells. BioRxiv. 10.1101/2020.09.27.316117.
30. Cai D, Chen S-C, Prasad M, He L, Wang X, Choesmel-Cadamuro V, Sawyer JK, Danuser G, and Montell DJ (2014). Mechanical feedback through E-cadherin promotes direction sensing during collective cell migration. Cell 157, 1146–1159. 10.1016/j.cell.2014.03.045. [PubMed: 24855950]
31. Qin L, Yang D, Yi W, Cao H, and Xiao G (2021). Roles of leader and follower cells in collective cell migration. Mol. Biol. Cell 32, 1267–1272. 10.1091/mbc.E20-10-0681. [PubMed: 34184941]
32. Inaki M, Vishnu S, Cliffe A, and Rørth P (2012). Effective guidance of collective migration based on differences in cell states. Proc Natl Acad Sci USA 109, 2027–2032. 10.1073/pnas.1115260109. [PubMed: 22308382]
33. Wang H, Qiu Z, Xu Z, Chen SJ, Luo J, Wang X, and Chen J (2018). aPKC is a key polarity determinant in coordinating the function of three distinct cell polarities during collective migration. Development 145. 10.1242/dev.158444.
34. Cooke M, Kreider-Letterman G, Baker MJ, Zhang S, Sullivan NT, Eruslanov E, Abba MC, Goicoechea SM, García-Mata R, and Kazanietz MG (2021). FARP1, ARHGEF39, and TIAM2

are essential receptor tyrosine kinase effectors for Rac1-dependent cell motility in human lung adenocarcinoma. Cell Rep. 37, 109905. 10.1016/j.celrep.2021.109905. [PubMed: 34731623]

35. Takegahara N, Kang S, Nojima S, Takamatsu H, Okuno T, Kikutani H, Toyofuku T, and Kumanogoh A (2010). Integral roles of a guanine nucleotide exchange factor, FARP2, in osteoclast podosome rearrangements. FASEB J. 24, 4782–4792. 10.1096/fj.10-158212. [PubMed: 20702777]
36. Elbediwy A, Zhang Y, Cobbaut M, Riou P, Tan RS, Roberts SK, Tynan C, George R, Kjaer S, Martin-Fernandez ML, et al. (2019). The Rho family GEF FARP2 is activated by aPKCι to control tight junction formation and polarity. J. Cell Sci. 132. 10.1242/jcs.223743.
37. Godt D, and Tepass U (2009). Breaking a temporal barrier: signalling crosstalk regulates the initiation of border cell migration. Nat. Cell Biol. 11, 536–538. 10.1038/ncb0509-536. [PubMed: 19404334]
38. Pinheiro EM, and Montell DJ (2004). Requirement for Par-6 and Bazooka in Drosophila border cell migration. Development 131, 5243–5251. 10.1242/dev.01412. [PubMed: 15456726]
39. Szafranski P, and Goode S (2004). A Fasciclin 2 morphogenetic switch organizes epithelial cell cluster polarity and motility. Development 131, 2023–2036. 10.1242/dev.01097. [PubMed: 15056617]
40. Zhao M, Szafranski P, Hall CA, and Goode S (2008). Basolateral junctions utilize warts signaling to control epithelial-mesenchymal transition and proliferation crucial for migration and invasion of Drosophila ovarian epithelial cells. Genetics 178, 1947–1971. 10.1534/genetics.108.086983. [PubMed: 18430928]
41. Li Q, Feng S, Yu L, Zhao G, and Li M (2011). Requirements of Lgl in cell differentiation and motility during Drosophila ovarian follicular epithelium morphogenesis. Fly (Austin) 5, 81–87. 10.4161/fly.5.2.14436. [PubMed: 21245664]
42. Betschinger J, Mechtler K, and Knoblich JA (2003). The Par complex directs asymmetric cell division by phosphorylating the cytoskeletal protein Lgl. Nature 422, 326–330. 10.1038/nature01486. [PubMed: 12629552]
43. Goode S, and Perrimon N (1997). Inhibition of patterned cell shape change and cell invasion by Discs large during Drosophila oogenesis. Genes Dev. 11, 2532–2544. [PubMed: 9334318]
44. Goode S, Wei J, and Kishore S (2005). Novel spatiotemporal patterns of epithelial tumor invasion in Drosophila discs large egg chambers. Dev. Dyn. 232, 855–864. 10.1002/dvdy.20336. [PubMed: 15712204]
45. Manseau L, Baradaran A, Brower D, Budhu A, Elefant F, Phan H, Philp AV, Yang M, Glover D, Kaiser K, et al. (1997). GAL4 enhancer traps expressed in the embryo, larval brain, imaginal discs, and ovary of drosophila. Developmental Dynamics.
46. Colombié N, Choesmel-Cadamuro V, Series J, Emery G, Wang X, and Ramel D (2017). Non-autonomous role of Cdc42 in cell-cell communication during collective migration. Dev. Biol. 423, 12–18. 10.1016/j.ydbio.2017.01.018. [PubMed: 28143705]
47. Plutoni C, Keil S, Zeledon C, Delsin LEA, Decelle B, Roux PP, Carréno S, and Emery G (2019). Misshapen coordinates protrusion restriction and actomyosin contractility during collective cell migration. Nat. Commun. 10, 3940. 10.1038/s41467-019-11963-7. [PubMed: 31477736]
48. Bonello TT, and Peifer M (2019). Scribble: A master scaffold in polarity, adhesion, synaptogenesis, and proliferation. J. Cell Biol. 218, 742–756. 10.1083/jcb.201810103. [PubMed: 30598480]
49. Harmansa S, Alborelli I, Bieli D, Caussinus E, and Affolter M (2017). A nanobody-based toolset to investigate the role of protein localization and dispersal in Drosophila. eLife 6. 10.7554/eLife.22549.
50. Theveneau E, and Linker C (2017). Leaders in collective migration: are front cells really endowed with a particular set of skills? [version 1; peer review: 2 approved]. F1000Res. 6, 1899. 10.12688/f1000research.11889.1. [PubMed: 29152225]
51. Haney S, Konen J, Marcus AI, and Bazhenov M (2018). The complex ecosystem in non small cell lung cancer invasion. PLoS Comput. Biol. 14, e1006131. 10.1371/journal.pcbi.1006131. [PubMed: 29795571]
52. Cheung KJ, Padmanaban V, Silvestri V, Schipper K, Cohen JD, Fairchild AN, Gorin MA, Verdone JE, Pienta KJ, Bader JS, et al. (2016). Polyclonal breast cancer metastases arise from collective

dissemination of keratin 14-expressing tumor cell clusters. Proc Natl Acad Sci USA 113, E854–63. 10.1073/pnas.1508541113. [PubMed: 26831077]

53. Conod A, Silvano M, and Ruiz I Altaba A (2022). On the origin of metastases: Induction of pro-metastatic states after impending cell death via ER stress, reprogramming, and a cytokine storm. Cell Rep. 38, 110490. 10.1016/j.celrep.2022.110490. [PubMed: 35263600]
54. Bhatia A (2013). Why are these caterpillars climbing over each other? The surprising science behind the swarm. | WIRED. https://www.wired.com/2013/07/why-are-these-caterpillars-climbing-over-each-other-the-surprising-science-behind-the-swarm/.
55. Prasad M, and Montell DJ (2007). Cellular and molecular mechanisms of border cell migration analyzed using time-lapse live-cell imaging. Dev. Cell 12, 997–1005. 10.1016/j.devcel.2007.03.021. [PubMed: 17543870]
56. Sano H, Ricardo S, and Lehmann R (2007). Tumbling, an interactive way to move forward. Sci. STKE 2007, pe63. 10.1126/stke.4122007pe63. [PubMed: 18000236]
57. Fulga TA, and Rørth P (2002). Invasive cell migration is initiated by guided growth of long cellular extensions. Nat. Cell Biol. 4, 715–719. 10.1038/ncb848. [PubMed: 12198500]
58. Rørth P (2009). Collective cell migration. Annu. Rev. Cell Dev. Biol. 25, 407–429. 10.1146/annurev.cellbio.042308.113231. [PubMed: 19575657]
59. Mishra AK, Mondo JA, Campanale JP, and Montell DJ (2019). Coordination of protrusion dynamics within and between collectively migrating border cells by myosin II. Mol. Biol. Cell 30, 2490–2502. 10.1091/mbc.E19-02-0124. [PubMed: 31390285]
60. Zegers MM, and Friedl P (2014). Rho GTPases in collective cell migration. Small GTPases 5, e28997. 10.4161/sgtp.28997. [PubMed: 25054920]
61. Condeelis J (1993). Understanding the cortex of crawling cells: insights from Dictyostelium. Trends Cell Biol. 3, 371–376. 10.1016/0962-8924(93)90085-f. [PubMed: 14731653]
62. Stossel TP (1993). On the crawling of animal cells. Science 260, 1086–1094. 10.1126/science.8493552. [PubMed: 8493552]
63. Small JV, Anderson K, and Rottner K (1996). Actin and the coordination of protrusion, attachment and retraction in cell crawling. Biosci. Rep. 16, 351–368. [PubMed: 8913526]
64. Hecht I, Skoge ML, Charest PG, Ben-Jacob E, Firtel RA, Loomis WF, Levine H, and Rappel W-J (2011). Activated membrane patches guide chemotactic cell motility. PLoS Comput. Biol. 7, e1002044. 10.1371/journal.pcbi.1002044. [PubMed: 21738453]
65. Bershadsky AD, and Kozlov MM (2011). Crawling cell locomotion revisited. Proc Natl Acad Sci USA 108, 20275–20276. 10.1073/pnas.1116814108. [PubMed: 22159034]
66. Friedl P, and Wolf K (2010). Plasticity of cell migration: a multiscale tuning model. J. Cell Biol. 188, 11–19. 10.1083/jcb.200909003. [PubMed: 19951899]
67. Montell DJ (2021). EMT, one of many morphological transitions in cellular phase space. Methods Mol. Biol. 2179, 13–18. 10.1007/978-1-0716-0779-4_3. [PubMed: 32939709]
68. Brumby AM, and Richardson HE (2003). scribble mutants cooperate with oncogenic Ras or Notch to cause neoplastic overgrowth in Drosophila. EMBO J. 22, 5769–5779. 10.1093/emboj/cdg548. [PubMed: 14592975]
69. Hariharan IK, and Bilder D (2006). Regulation of imaginal disc growth by tumor-suppressor genes in Drosophila. Annu. Rev. Genet. 40, 335–361. 10.1146/annurev.genet.39.073003.100738. [PubMed: 16872256]
70. Bilder D, Li M, and Perrimon N (2000). Cooperative regulation of cell polarity and growth by Drosophila tumor suppressors. Science 289, 113–116. 10.1126/science.289.5476.113. [PubMed: 10884224]
71. Wu M, Pastor-Pareja JC, and Xu T (2010). Interaction between Ras(V12) and scribbled clones induces tumour growth and invasion. Nature 463, 545–548. 10.1038/nature08702. [PubMed: 20072127]
72. Igaki T, Pagliarini RA, and Xu T (2006). Loss of cell polarity drives tumor growth and invasion through JNK activation in Drosophila. Curr. Biol. 16, 1139–1146. 10.1016/j.cub.2006.04.042. [PubMed: 16753569]
73. Pagliarini RA, and Xu T (2003). A genetic screen in Drosophila for metastatic behavior. Science 302, 1227–1231. 10.1126/science.1088474. [PubMed: 14551319]

74. Lin W-H, Asmann YW, and Anastasiadis PZ (2015). Expression of polarity genes in human cancer. Cancer Inform. 14, 15–28. 10.4137/CIN.S18964. [PubMed: 25991909]

75. Santoni M-J, Kashyap R, Camoin L, and Borg J-P (2020). The Scribble family in cancer: twentieth anniversary. Oncogene 39, 7019–7033. 10.1038/s41388-020-01478-7. [PubMed: 32999444]

76. Libanje F, Raingeaud J, Luan R, Thomas Z, Zajac O, Veiga J, Marisa L, Adam J, Boige V, Malka D, et al. (2019). ROCK2 inhibition triggers the collective invasion of colorectal adenocarcinomas. EMBO J. 38, e99299. 10.15252/embj.201899299. [PubMed: 31304629]

77. Harrison DA, and Perrimon N (1993). Simple and efficient generation of marked clones in Drosophila. Curr. Biol. 3, 424–433. 10.1016/0960-9822(93)90349-s. [PubMed: 15335709]

78. Kardash E, Bandemer J, and Raz E (2011). Imaging protein activity in live embryos using fluorescence resonance energy transfer biosensors. Nat. Protoc. 6, 1835–1846. 10.1038/nprot.2011.395. [PubMed: 22051797]

79. Albertson R, and Doe CQ (2003). Dlg, Scrib and Lgl regulate neuroblast cell size and mitotic spindle asymmetry. Nat. Cell Biol. 5, 166–170. 10.1038/ncb922. [PubMed: 12545176]

80. McDonald JA, Khodyakova A, Aranjuez G, Dudley C, and Montell DJ (2008). PAR-1 kinase regulates epithelial detachment and directional protrusion of migrating border cells. Curr. Biol. 18, 1659–1667. 10.1016/j.cub.2008.09.041. [PubMed: 18976916]

81. Cho A, Kato M, Whitwam T, Kim JH, and Montell DJ (2016). An Atypical Tropomyosin in Drosophila with Intermediate Filament-like Properties. Cell Rep. 16, 928–938. 10.1016/j.celrep.2016.06.054. [PubMed: 27396338]

82. Schindelin J, Arganda-Carreras I, Frise E, Kaynig V, Longair M, Pietzsch T, Preibisch S, Rueden C, Saalfeld S, Schmid B, et al. (2012). Fiji: an open-source platform for biological-image analysis. Nat. Methods 9, 676–682. 10.1038/nmeth.2019. [PubMed: 22743772]

Highlights

- Follower border cells require Rac activity for actin dynamics and crawling behaviors
- Rac-dependent follower cell motility promotes cluster compactness and movement
- Basolateral Scrib, DLG, and LGL localize the GEF Cdep to activate Rac in followers
- The Scrib/Cdep/Rac pathway promotes follower cell crawling and cluster cohesion

Inclusion and diversity statement

- Some authors self-identify as a member of an underrepresented group.
- We acknowledge the exclusions and erasures of many Indigenous peoples, including those on whose lands the University of California, Santa Barbara is located, the villages and unceded territories of the Chumash people. We acknowledge the Chumash People, their Elders, both past and present, as well as their future generations.
- Efforts for balanced, equitable, and gender-unbiased citing were made throughout the development of this manuscript.

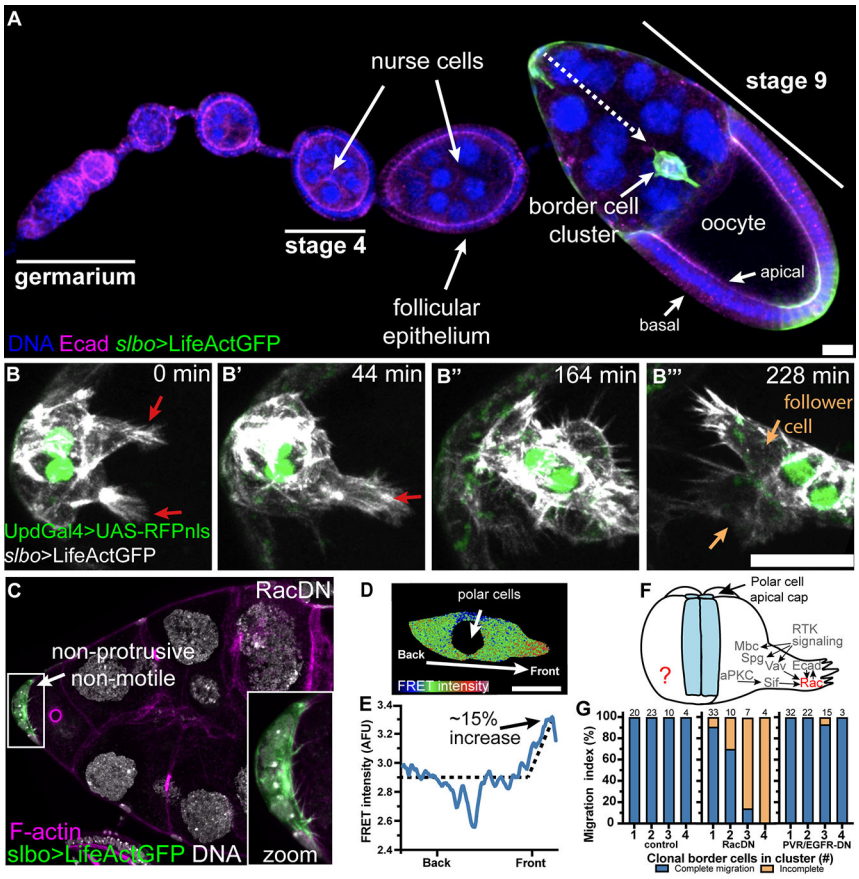

Figure 1: Rac is required in follower cells.

(A) Projected *Drosophila* ovariole from the ovary with DNA (blue), Ecad (magenta), and *slbo*>LifeActinGFP (green). (B-B"') Stills from a time-lapse of delaminating border cells expressing *slbo*>LifeActGFP (white) and polar cell nuclei expressing *upd*Gal4>UAS-RFPnls (green). Lead cell protrusions and follower cells are marked by red and orange arrows, respectively. (C) Inhibition of Rac in all border cells blocks protrusion and migration. (D) Intensity coded RacFRET signal co-expressing control UAS-*w*RNAi. (E) Line plot of RacFRET intensity for cluster in (D). (F) Border cell cluster schematic overlayed with known Rac signaling in lead cell protrusions. (G) Frequency distribution for complete border cell migration of clusters containing variable numbers of clonal cells expressing the indicated UAS transgene. Number of clusters counted are indicated on top of the histogram. All scale bars are 20 μm.

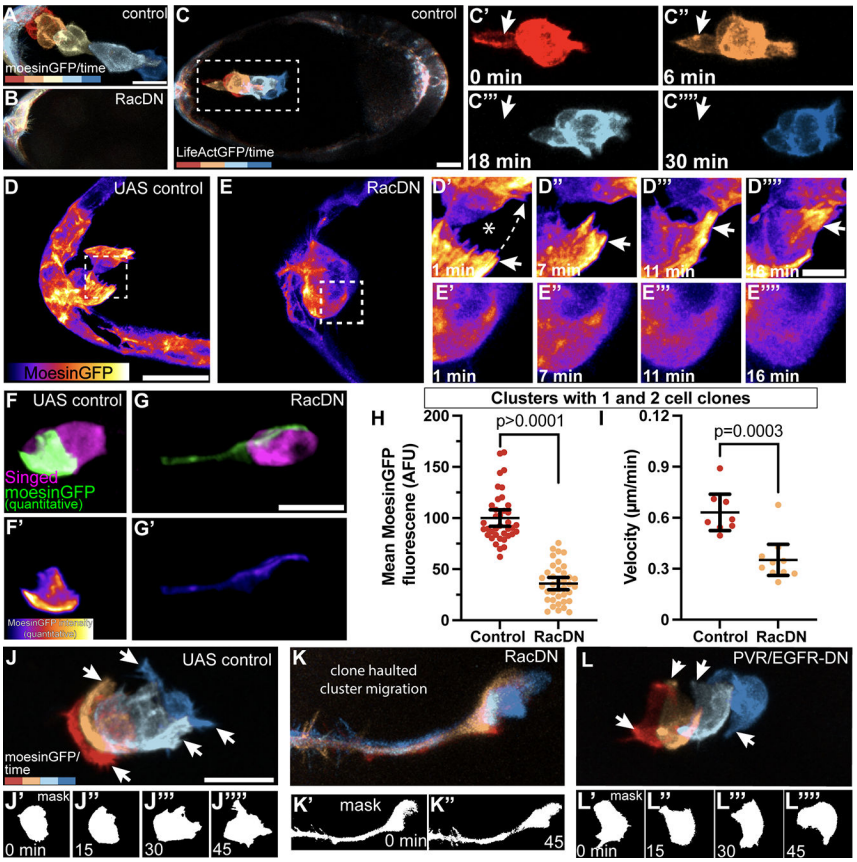

Figure 2: Rac is required in follower cells for actin dynamics, shape changes, and motility.

(A, B) Time color-coded images from movies for (A) wild type and (B) Rac-inhibited border cells (see Movie 2). (C) Time color-coded still images (C'-C"") from a time lapse movie (Movie 3) of a wild type cluster showing that follower cell motility promotes cluster compactness. (D-E) Intensity color-coded live imaging of AyFLPout clones at time zero expressing UAS-moesinGFP and co-expressing either (D) UAS-*w*RNAi showing a follower cell crawling over another border cell (* in D') or (E) UAS-RacDN, showing that Rac is required for follower cell crawling. D'-D"" and E'-E"" zooms of the boxed regions in D and E, respectively. Arrows mark protrusions from crawling follower cells on an unmarked cell (*= unmarked cell, dashed line= approximate cell boundary). (F-G) Single border cell clones expressing UAS-moesinGFP (green) and either (F) UAS-*w*RNAi or (G) UAS-RacDN, marked with Singed (magenta). GFP in (F) and (G) and (F' and G') show quantitative GFP fluorescence. (H) Quantitation of moesinGFP from (F and G). Each dot is one clone. (I) Quantification of border cell cluster migration velocity containing clonal cells. Each dot is one cluster. (J-L) Time color-coded images from movies for follower cell clones expressing (J) UAS-wRNAi, (K) UAS-RacDN, or (L), UAS-PVR/EGFR-DNs. Arrows indicate dynamic protrusions changing between timepoints. (J'-L"'). Masks showing shape changes of clones in (J-L) over time. All scale bars= 20 µm except D'-D"' and E'-E"' which are 10 µm. Statistical significance tested using unpaired t-test.

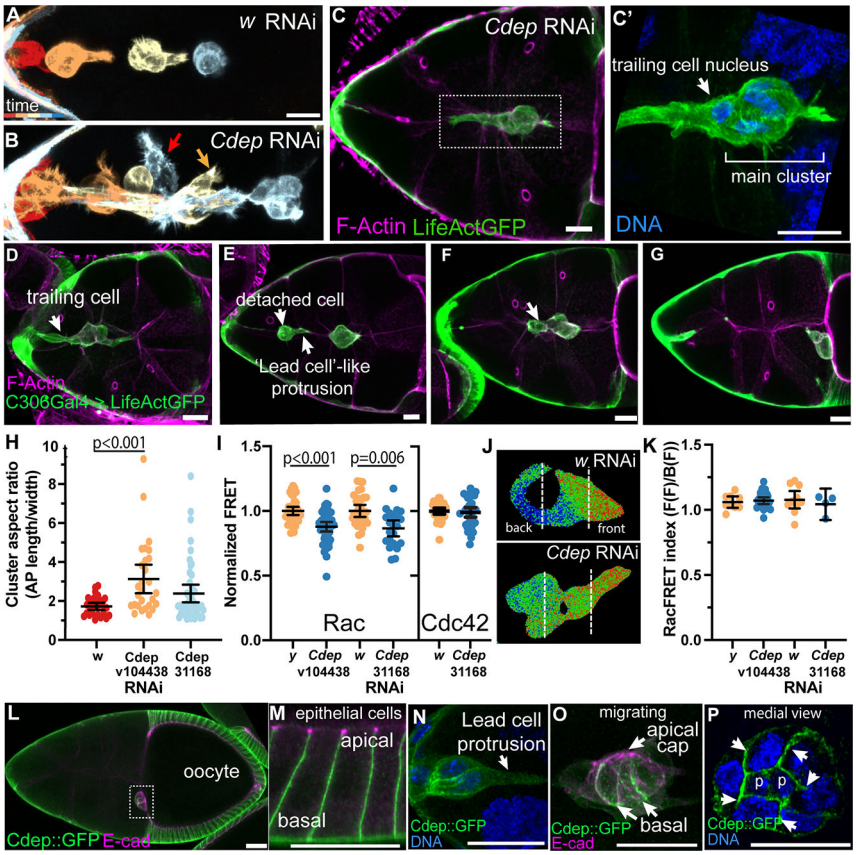

Figure 3: The basally localized RacGEF, Cdep, is required for follower cell crawling behavior and cluster cohesion.

(A-B) 30 min interval color coded images from 3.5 hr time lapse movies for RNAi indicated. Red arrow indicates a detached border cell, and orange arrow indicates ectopic protrusion. (C-G) Representative projections of border cell clusters expressing UAS-*Cdep*RNAi stained for F-actin (magenta) and slbo>LifeActGFP (green). (C-D) trailing cells, (E) single cells falling off the cluster, (F-G) loss of cohesion. (H) Dot plot of cluster aspect ratio. Each dot is one cluster. (I) Analysis of c306Gal4, UAS-RacFRET or UAS-Cdc42FRET intensities and co-expressing control UAS-*w*RNAi/UAS-*y*RNAi or UAS-*Cdep*RNAi. Each dot is one cluster. (J) Representative images of RacFRET. (K) Front/back RacFRET intensity ratio of protrusive clusters in (I). (L) Projection of stage 10 egg chamber stained for Cdep::GFP (green) and Ecadherin (magenta). Dashed box indicates docked border cell cluster. (M) Zoom of epithelial follicle cells. (N) Delaminating border cells stained for Cdep (green). (O) Migrating border cell cluster stained as in (L). (P) Medial view of a border cell cluster with arrows marking border/border cell boundaries and “p” marking polar cell nuclei. All scale bars= 20 μm. Statistical significance tested using one-way ANOVA with Kruskal-Wallace (H) and Tukey (I and K) post hoc analysis.

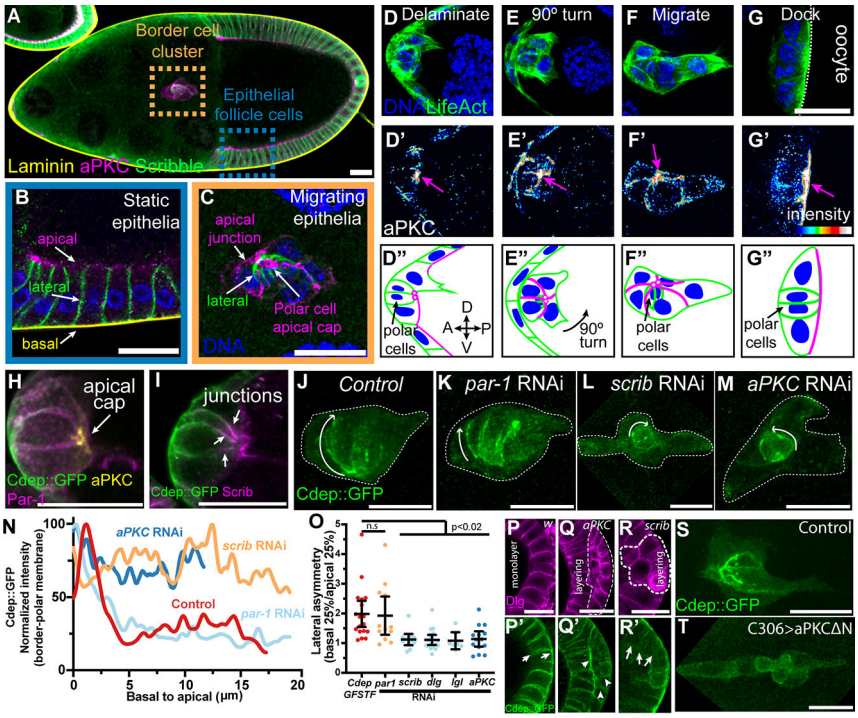

Figure 4: Core polarity modules localize Cdep in border cell clusters.

(A) Projected stage 9 egg chamber with migrating border cells stained for Laminin with peanut lectin (yellow), aPKC on apical membrane (magenta), and Scribble on lateral membrane (green). (B) Epithelial follicle cell and (C) border cell zooms of (A) with DNA (blue). (D-G") Stages of border cell migration from stage 9–10 egg chambers with DNA (blue), (D-G) Actin staining from *slbo*>LifeActinGFP reporter (green), (D'-G') aPKC staining (color coded by intensity) with arrows to denote the apical cap of the polar cells, and (D"-G") schematic representations of D-G'. Axis in D" indicates anterior, A, posterior, P, dorsal, D, and ventral, V. (H) Overlay of a border cell cluster stained for endogenous Cdep::GFP (green), Par-1 (magenta), and aPKC (yellow). (I) Overlay of a border cell cluster stained for Cdep::GFP (green), and Scribble (magenta). (J-M) Representative images of border cell clusters expressing Cdep::GFP in combination with indicated RNAi. Arrow points toward apical. (N) Representative line scans along the polar/border cell boundary from basal to apical for genotypes in (J-M). (O) Dot plot of basal to apical asymmetry of Cdep at polar/border cell membrane for indicated knockdowns. Each dot is an individual border cell cluster. Statistical significance was tested using one-way ANOVA with Kruskal-Wallace post hoc. (P-R') Representative images of Dlg (magenta) and Cdep::GFP (green) in control (P,P'), *aPKC* RNAi (Q-Q') and *scrib* RNAi (R-R'). Layering is outlined. (S) Control and (T) UAS-aPKCΔN expressing border cell clusters during migration. All scale bars= 20 μm.

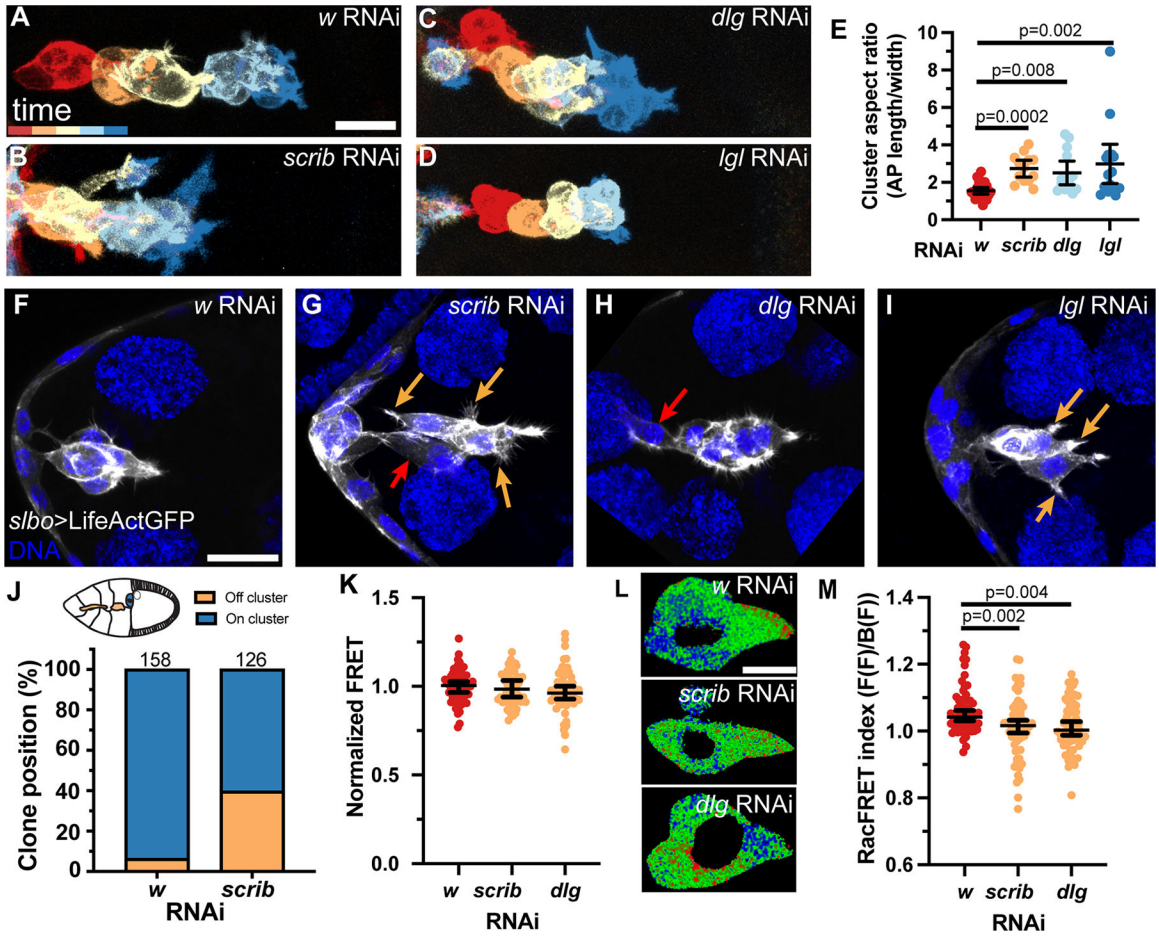

Figure 5. The Scrib module coordinates cluster cohesion, detachment, and migration dynamics.

(A-D) Representative projections of migrating border cell clusters expressing c306Gal4, *slbo*>LifeActGFP, *tub*Gal80^{ts}, and indicated UAS-RNAi in 30 min interval color coded images from 4 hr time lapse movies for RNAi indicated. (E) Dot plot of cluster aspect ratio. Each dot is one cluster. (F-I) Representative projections of migrating border cell clusters for indicated UAS-RNAi. LifeAct (white) and DNA (blue). Cells with ectopic protrusions or that fell off the cluster marked with orange or red arrows, respectively. (J) Schematic and proportion of stage 10 egg chambers with clonal border cells on or off the cluster expressing the indicated UAS-RNAi under the control of HsFlp>AyGal4. Number of egg chambers counted at top of histogram. (K) Analysis of c306Gal4, UAS-RacFRET intensities and co-expressing indicated RNAi. Each dot is one cluster. (L) Representative images of RacFRET. (M) Front/back RacFRET intensity ratio of clusters in (K). All scale bars= 20μm. Statistical significance tested using one-way ANOVA with Kruskal-Wallace post hoc analysis.

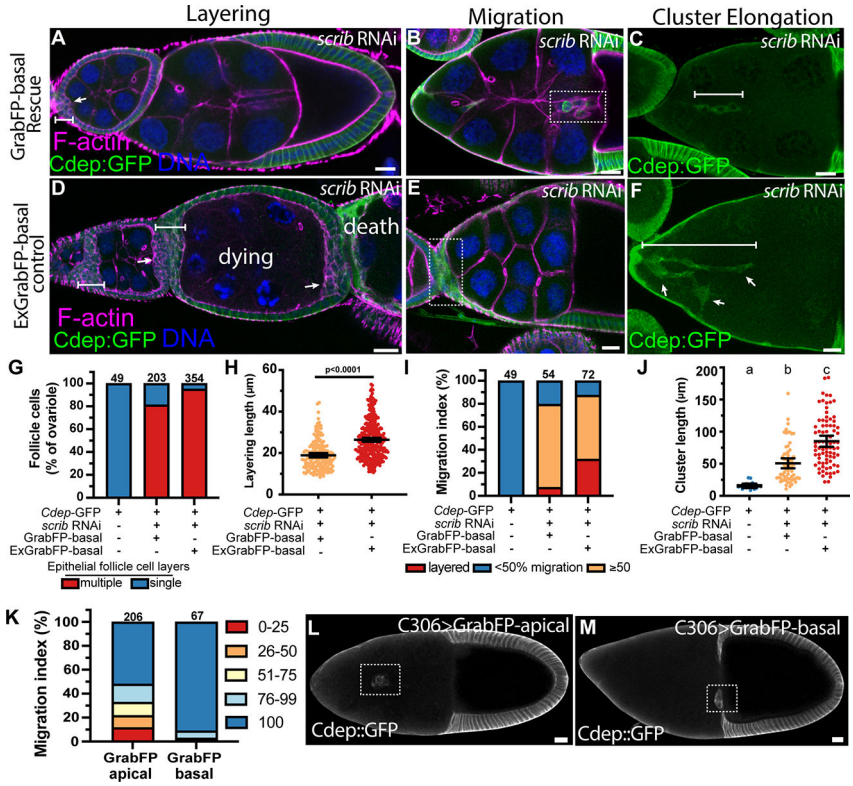

Figure 6: Re-localizing Cdep to the basal membrane suppresses border cell epithelial layering and cluster elongation caused by Scrib module knockdown.

(A-F) Egg chambers expressing (A-C) UAS-GrabFP-basal or (D-F) UAS-ExGrabFP-basal and co-expressing UAS-Scrib RNAi, stained for F-actin (magenta), Cdep::GFP (green), and DNA (blue). (A and D) Layering throughout the egg chamber (arrow). Bars represent the length measurement for anterior layering. (B and E) Dotted box indicates the border cell cluster. (C and F) Bar represents the length measurement for cluster elongation. (G) Quantification of ovariole strands where either no layering was observed (blue), or any layering (red) anywhere within a single ovariole strand. Number of ovarioles counted at top of histogram. (H) Quantification of anterior layering size. Each dot is on cluster. (I) Frequency distribution of migration defects in stage 10 egg chambers. Number of clusters counted on top of histogram. (J) Quantification of cluster elongation as the length of the longest line that can be drawn through the anterior-posterior axis of the border cell cluster. Each dot is one cluster. (K) Frequency distribution of migration defects in stage 10 egg chambers. Number of clusters counted on top of histogram. (L-M) Representative stage 10 Cdep::GFP egg chambers expressing (L) UAS-GrabFP-apical or (M) UAS-GrabFP-basal under the control of C306Gal4. Statistical significance was tested using one-way ANOVA with Kruskal-Wallace post hoc analysis. All scale bars= 20 µm.

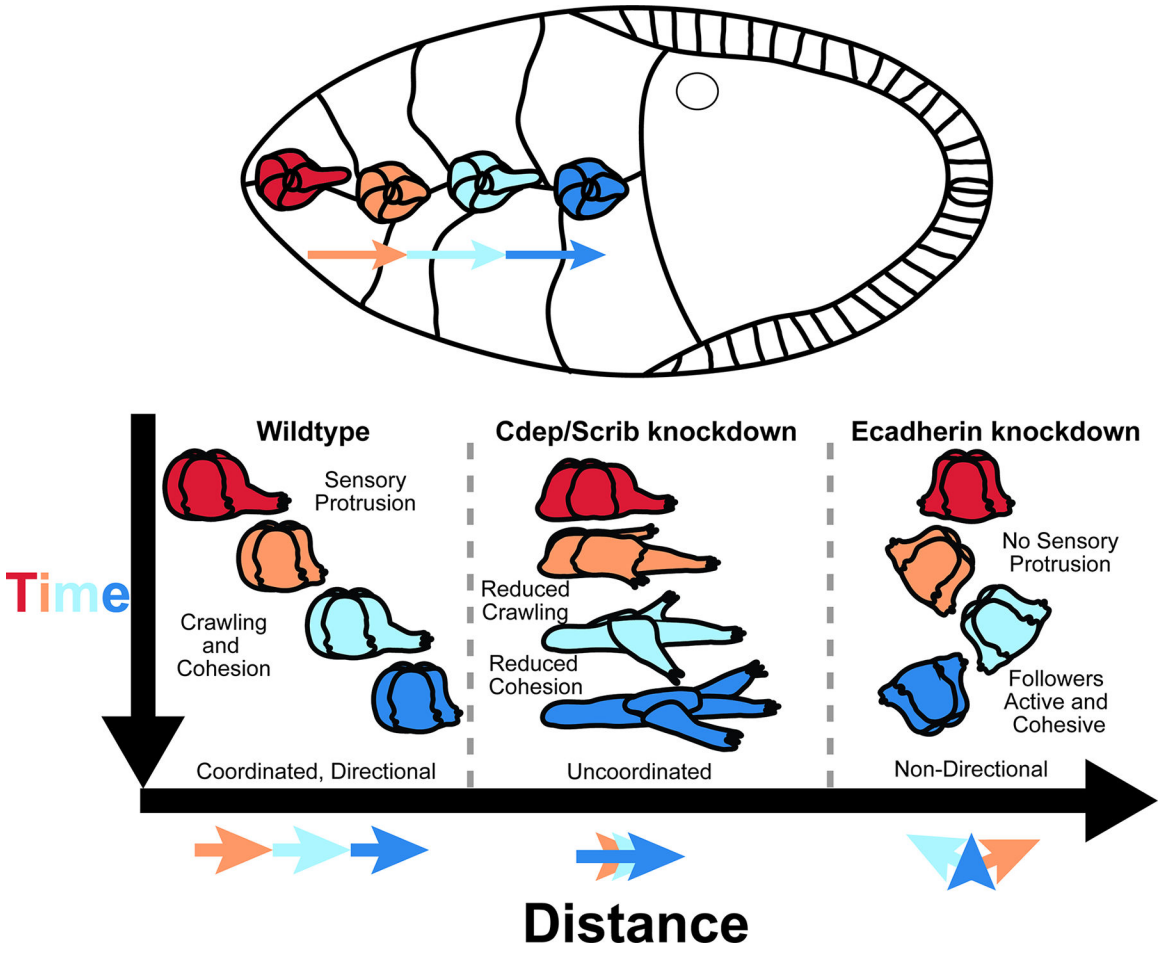

Figure 7: An integrated view of collective border cell migration.

Illustration of wild type border cell cluster migration. Color indicates sequential time points. Comparison of features of normal border cell leader and follower cell behaviors and cluster movement to those of Cdep or Scrib knockdown and the complementary defects caused by Ecadherin knockdown (based on Cai et al., 2014, Movie S2). In wild type, the front cell extends a large protrusion that senses chemoattractants (Duchek and Rørth, 2000; Duchek et al., 2001; McDonald et al., 2004) and small spaces (Dai et al., 2020) and is shaped and stabilized by E-cadherin-mediated adhesion (Cai et al., 2014) and steers the cluster. Cluster cohesion and movement also require basal, Rac-dependent follower cell crawling. Knockdown of Cdep or Scrib disrupts crawling and thus cluster cohesion and coordinated movement. E-cadherin knockdown causes loss of lead cell protrusion and directional migration but cells within the cluster remain active and thereby maintain cohesion but exhibit random movement.

KEY RESOURCES TABLE

REAGENT or RESOURCE	SOURCE	IDENTIFIER
Antibodies		
Monoclonal rat anti-Ecadherin (1:50 dilution)	Developmental Studies Hybridoma Bank	Cat#DCAD2; RRID:AB_528120
Monoclonal mouse anti-Singed (Fascin) (1:50 dilution)	Developmental Studies Hybridoma Bank	Cat#sn 7c; RRID:AB_52823
Polyclonal rabbit anti-GFP (1:1000 dilution)	ThermoFisher Scientific	Cat#A-11122; RRID:AB_221569
Monoclonal mouse anti-aPKCzeta (1:500)	Santa Cruz Biotechnology	Cat#sc-17781 RRID:AB_628148
Polyclonal rabbit anti-Scribble	See Albertson and Doe, 2003 (79)	N/A
Polyclonal rabbit anti-Par-1	See McDonald et al., 2008 (80)	N/A
Monoclonal mouse anti-discs large (1:100)	Developmental Studies Hybridoma Bank	Cat#4F3; RRID:AB_528203
Polyclonal rabbit anti-Lgl (1:500)	Santa Cruz Biotechnology	Cat#sc-98260 RRID:AB_1564606
Monoclonal mouse anti-Cut (1:100 dilution)	Developmental Studies Hybridoma Bank	Cat#2b10; RRID:AB_528186
Chemicals, peptides, and recombinant proteins		
Hoechst 33342	Sigma-Aldrich	Cat#14533
Phalloidin Atto647N	Sigma-Aldrich	Cat#65906
Lectin PNA From *Arachis hypogaea* (peanut), Alexa Fluor™ 647 Conjugate	ThermoFisher Scientific	Cat#L32460
TritonX-100	Sigmal-Aldrich	Cat#T8787
Schneider's Drosophila Medium	Gibco	Cat#21720
Phosphate Buffered Saline (10x, pH 7.4)	Quality Biological	Cat#119-069-131
Paraformaldehyde, 16% solution	Electron Microscopy Sciences	Cat#15710
Vectasheild antifade mounting medium	Vector Laboratories	Cat#H-1000
Antibiotic-Antimycotic (100X)	ThermoFisher Scientific	Cat#15240062
Insulin (bovine pancreas)	Sigma-Aldrich	Cat#I1882
SeaPlaque Agarose	Lonza	Cat#50101
Experimental models: Organisms/strains		
D. melanogaster: w[1118]	Denise Montell Lab Stock, University of California Santa Barbara	N/A
D. melanogaster: w[*]; P{w[+mC]=tubP-GAL80[ts]}10; TM2/TM6B, Tb[1]	Bloomington Drosophila Stock Center	Cat#BDSC_7108, FBti0027799
D. melanogaster: w[*]; P{w[+mC]=slbo-Lifeact-GFP}2M/CyO; MKRS/TM6B, Tb[1]	See Cai et al., 2014 (30)	Cat#BDSC_58364, FBti0163120
D. melanogaster: upd-Gal4	See Cai et al., 2014 (30); gift from Douglas Harrison, University of Kentucky	N/A
D. melanogaster: P{w[+mC]=UAS-RedStinger}3, w[1118]	Bloomington Drosophila Stock Center	Cat#BDSC_8545 FBgn0044485
D. melanogaster: w[*]; sna[Sco]/CyO; P{w[+mC]=UAS-YPet-PAK-RAC-CFP.FRET}3	Bloomington Drosophila Stock Center	Cat#BDSC_31431 FBti0130032
D. melanogaster: w[*]; P{w[+mC]=UAS-YPet-PAK-RAC-CFP.FRET}2; MKRS/TM6B, Tb[1]	Bloomington Drosophila Stock Center	Cat#BDSC_32050 FBti0130028

REAGENT or RESOURCE	SOURCE	IDENTIFIER
D. melanogaster: hsp70-FLP; Ay17bGal4, UAS-moesin-GFP	Cho et al., 2016 (81)	NA
D. melanogaster: P{w[+mW.hs]=GawB}c306, w[1118]	Bloomington Drosophila Stock Center	Cat#BDSC_3743 FBti0003935
D. melanogaster: y[1] w[*]; P{w[+mC]=UAS-Rac1.N17}1	Bloomington Drosophila Stock Center	Cat#BDSC_6292 FBti0017573
D. melanogaster RNAi of *white*: y[1] v[1]; P{y[+t7.7] v[+t1.8]=TRiP.HMS00017}attP2	Bloomington Drosophila Stock Center	Cat#BDSC_33623 FBti0140096
D. melanogaster RNAi of *Cdep*: y[1] v[1]; P{y[+t7.7] v[+t1.8]=TRiP.JF01661}attP2	Bloomington Drosophila Stock Center	Cat#BDSC_31168 FBti0131039
D. melanogaster RNAi of *Cdep*: P(KK 108821)	Vienna Drosophila Resource Center	Cat#VDRC_ID_104438
D. melanogaster: w[*]; P{w[+mC]=UAS-YPet-PAK-Cdc42-CFP.FRET}2; MKRS/TM6B, Tb[1]	Denise Montell Lab Stock, University of California Santa Barbara	N/A
D. melanogaster: y[1] w[*]; Mi{PT-GFSTF.1}Cdep[MI06830-GFSTF.1]	Bloomington Drosophila Stock Center	Cat#BDSC_61789 FBti0178623
D. melanogaster RNAi of *Par-1*: P(GD 14836)	Vienna Drosophila Resource Center	Cat#VDRC_ID_52556
D. melanogaster RNAi of *scrib*: w[*]; P{w+mC]=UAS-scrib.RNAi}7L	Bloomington Drosophila Stock Center	Cat#BDSC_59080 FBti0166976
D. melanogaster RNAi of *aPKC*: P(KK 100874)	Vienna Drosophila Resource Center	Cat#VDRC_ID_105624
D. melanogaster: w[*]; P{w[+mC]=UAS-aPKC.DeltaN}3	Bloomington Drosophila Stock Center	Cat#BDSC_51673 FBti0154819
D. melanogaster RNAi of *scrib*: y[1] v[1]; P{y[+t7.7] v[+t1.8]=TRiP.JF03229}attP2	Bloomington Drosophila Stock Center	Cat#BDSC_29552 FBti0128927
D. melanogaster RNAi of dlg: P(GD 4689)	Vienna Drosophila Resource Center	Cat#VDRC_ID_41136
D. melanogaster RNAi of dlg: y[1] sc[*] v[1] sev[21]; P{y[+t7.7] v[+t1.8]=TRiP.JF01694}attP2	Bloomington Drosophila Stock Center	Cat#BDSC_31181 FBti0131052
D. melanogaster RNAi of lgl: P(GD 4047)	Vienna Drosophila Resource Center	Cat#VDRC_ID_51249
D. melanogaster RNAi of lgl: y[1] sc[*] v[1] sev[21]; P{y[+t7.7] v[+t1.8]=TRiP.HMS01522}attP2	Bloomington Drosophila Stock Center	Cat#BDSC_35773 FBti0145041
D. melanogaster GrabFP: w[*]; Kr[If-1]/CyO; M{w[+mC]=lexAop-UAS-GrabFP.B.Int.mCh}ZH-86Fb	Bloomington Drosophila Stock Center	Cat#BDSC_68175 FBti0187202
D. melanogaster GrabFP: w[*]; M{w[+mC]=lexAop-UAS-GrabFP.B.Ext.TagBFP}ZH-35B/CyO; TM3, Sb[1]/TM6B, Tb[1]	Bloomington Drosophila Stock Center	Cat#BDSC_68173 FBti0187199
Software and algorithms		
ImageJ2 (FIJI)	See Schindelin et al., 2012 (82) (https://fiji.sc)	N/A
Adobe Illustrator 2022	Adobe (https://www.adobe.com)	N/A
Imaris 9	Bitplane (https://imaris.oxinst.com)	N/A
Prism 9	Graph Pad	N/A